ACS Catalysis
Research Article
pubs.acs.org/acscatalysis

Amorphous Molybdenum Sulfide Catalysts for Electrochemical Hydrogen Production: Insights into the Origin of their Catalytic Activity

Jesse D. Benck, Zhebo Chen, Leah Y. Kuritzky, Arnold J. Forman, and Thomas F. Jaramillo*

Department of Chemical Engineering, Stanford University, 381 North-South Mall, Stanford, California 94305, United States

Supporting Information

ABSTRACT: We present a scalable wet chemical synthesis for a catalytically active nanostructured amorphous molybdenum sulfide material. The catalyst film is one of the most active nonprecious metal materials for electrochemical hydrogen evolution, drawing 10 mA/cm^2 at ~200 mV overpotential. To identify the active phase of the material, we perform X-ray photoelectron spectroscopy after testing under a variety of conditions. As deposited, the catalyst resembles amorphous MoS_3, but domains resembling MoS_2 in composition and chemical state are created under reaction conditions and may contribute to this material's high electrochemical activity. The activity scales with electrochemically active surface area, suggesting that the rough, nanostructured catalyst morphology also contributes substantially to the film's high activity. Electrochemical stability tests indicate that the catalyst remains highly active throughout prolonged operation. The overpotential required to attain a current density of 10 mA/cm^2 increases by only 57 mV after 10 000 reductive potential cycles. Our enhanced understanding of this highly active amorphous molybdenum sulfide hydrogen evolution catalyst may facilitate the development of economical electrochemical hydrogen production systems.

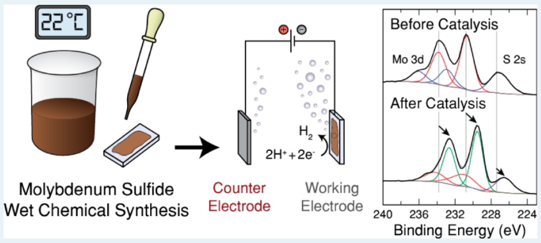

KEYWORDS: *electrocatalysis, molybdenum sulfide, hydrogen evolution, wet chemical synthesis, nanostructured film*

■ INTRODUCTION

Hydrogen, produced today mainly from natural gas or coal, is an extremely important chemical utilized at the global scale for major industrial processes, including petroleum refining and ammonia synthesis.[1,2] Hydrogen has also been proposed as a future energy carrier that could be used to power electronic devices, vehicles, and homes.[3,4] Developing methods to economically produce hydrogen from renewable energy resources could lead to substantial reductions in fossil fuel consumption and lower global CO_2 emissions.

A great deal of attention has recently been devoted to producing hydrogen from water through sustainable electrochemical processes such as photoelectrochemical water splitting or electrolysis driven by an external renewable source of electricity.[4−7] The hydrogen evolution reaction (HER), $2H^+ + 2e^- \rightarrow H_2$, is a fundamental component of water splitting. Achieving high energetic efficiency for water splitting requires the use of a catalyst to minimize the overpotential necessary to drive the HER.[5,8]

The best known catalysts for the HER are precious metals, such as platinum, ruthenium, and iridium, but the scarcity and high cost of these materials prohibit their wide-scale deployment.[5,9−11] Nickel alloy catalysts show high activity for the HER in alkaline electrolytes, but often degrade in acidic solutions.[12−19] The development of a scalable, environmentally friendly synthesis for an inexpensive, highly active, acid-stable HER catalyst remains a major challenge.[5,20−23]

Molybdenum sulfide materials have shown high activity and stability for the HER in acidic environments,[24−31] but previous procedures for synthesizing these catalysts have typically involved ultrahigh-vacuum processing,[32] high-temperature treatment,[27,28] sulfidization using H_2S gas,[27,32] or electrodeposition,[29] which could limit the range of potential applications. Recent work has revealed scalable procedures for synthesizing highly active amorphous molybdenum sulfide catalysts.[11,28,33,34] However, much remains to be learned about the properties of amorphous molybdenum sulfide and the origins of its catalytic activity.

Herein, we report a facile wet chemical synthesis for a nanostructured amorphous molybdenum sulfide catalyst and aim to understand the origin of its catalytic activity. The synthesis technique is based on readily available precursors; avoids the need for high-vacuum processing, high-temperature treatment, or a separate sulfidization step; and enables straightforward catalyst deposition onto a wide range of substrates. Physical and chemical characterization suggests that the resulting catalyst is similar to other recently reported amorphous MoS_3 materials in structure and composition, but this material currently has the highest reported activity of any molybdenum sulfide catalyst produced through a room

Received: February 26, 2012
Revised: July 25, 2012
Published: August 10, 2012

temperature wet chemical process. To understand the origin of this material's activity, we investigated changes in the catalyst morphology, composition, and activity during catalysis. These results suggest that the high activity of this material likely arises from both the inherently favorable surface properties of the active molybdenum sulfide phase and the rough, nanostructured catalyst film morphology. Having enhanced the understanding of this material's properties, we propose strategies for further improving its performance.

■ EXPERIMENTAL SECTION

Catalyst Synthesis. The molybdenum sulfide catalyst was prepared via a room temperature wet chemical synthesis. All reagents were purchased and used as received.

A molybdenum precursor solution was prepared by adding 0.60 g of ammonium heptamolybdate ($Mo_7O_{24}(NH_4)_6 \cdot 4H_2O$, Sigma-Aldrich) to 12 mL of 0.2 M sulfuric acid (H_2SO_4, Aldrich) in Millipore water (18 MΩ cm). In a second container, a sulfur precursor solution was prepared by adding 0.075 g of sodium sulfide (Na_2S, Alfa Aesar) to 12 mL of Millipore water. These two solutions were mixed, yielding a 24 mL solution of 0.02 M ammonium heptamolybdate, 0.04 M sodium sulfide, and 0.1 M sulfuric acid in water. Upon mixing the solutions, a suspension of nanoparticles was immediately formed. The suspension was centrifuged at 12 000 rpm (relative centrifugal force 17 400) for 30 min to collect the nanoparticles. After discarding the supernatant, the solid centrifuge pellet was rinsed once with 15 mL of isopropyl alcohol, and the rinsing liquid was discarded. The pellet was then redispersed in an additional 15 mL of isopropyl alcohol via sonication for 10 min to give the final catalyst solution used for drop-casting.

The catalyst samples with typical mass loading used for the scanning electron microscopy, X-ray photoelectron spectroscopy, Raman spectroscopy, and electrochemical testing were prepared by drop-casting 10 μL of the redispersed suspension onto 5-mm-diameter glassy carbon disks (Sigradur G, HTW Hochtemperatur-Werkstoffe GmbH). The sample used for X-ray diffraction analysis was prepared by drop-casting 2 mL of the redispersed suspension onto a 50 × 75 mm glass microscope slide. The sample used for transmission electron microscopy was prepared by diluting the sonicated nanoparticle suspension by 400× in isopropyl alcohol and drop-casting 2 μL of this mixture onto a holey carbon support (Ted Pella Catalogue no. 01824). A series of samples with mass loadings ranging from 400% to 25% of the typical preparation were synthesized by redispersing the solid pellet formed after centrifugation in 3.75 mL of isopropyl alcohol and using a 1:1 dilution series in isopropyl alcohol to make five solutions with 400%, 200%, 100%, 50%, and 25% of the typical catalyst concentration. A 10 μL aliquot of each solution was then deposited onto a 5 mm glassy carbon disk. All samples were dried under low vacuum (~25 Torr) for several hours prior to characterization.

Physical and Chemical Characterization. Scanning electron microscopy (SEM) was performed before and after electrochemical characterization using an FEI Magellan XHR microscope operated with a beam voltage of 5.0 kV and current of 25 pA. Transmission electron microscopy (TEM) of the catalyst was collected using an FEI Titan 80-300 microscope operated at 300 kV.

X-ray diffraction (XRD) spectra were collected using a PANalytical X'Pert Pro diffractometer with a Cu Kα X-ray source operated at 40 kV and 45 mA. X-ray photoelectron spectroscopy (XPS) was performed using a Phi VersaProbe spectrometer with an Al Kα source, and binding energies were calibrated to the adventitious C 1s peak at 284.6 eV. Raman spectra were collected using a Cobolt Blues 473 nm blue diode pumped solid state laser at ~1 mW and an Andor charge-coupled detector held at −50 °C with a thermoelectric cooling plate.

Electrochemical Characterization. Electrochemical measurements were performed in a three-electrode electrochemical cell in a rotating disk electrode (RDE) configuration with a Bio-Logic potentiostat (VMP3). All tests were performed in 80–100 mL of 0.5 M sulfuric acid (H_2SO_4) electrolyte prepared in Millipore water (18 MΩ cm) with a Hg/Hg_2SO_4 in saturated K_2SO_4 reference electrode (Hach) and a graphite rod counter electrode (Ted Pella). The molybdenum sulfide catalyst film on a glassy carbon disk was used as the working electrode. The reversible hydrogen electrode (RHE) was calibrated to between −0.700 V and −0.706 V vs the Hg/Hg_2SO_4 reference electrode as measured using platinum mesh working and counter electrodes under a H_2 gas purge. The potential scale was calibrated to RHE after each experiment to prevent contamination of the cell with platinum ions dissolved from the electrodes during this calibration step.

Prior to further characterization, the catalyst was electrochemically activated by performing approximately three potential cycles between 0.10 and −0.25 V vs RHE at 20 mV/s. After the initial stabilization of the activity, the performance of the catalyst for the hydrogen evolution reaction was measured using a linear sweep voltammogram beginning at the open circuit potential of ~0.30 V vs RHE and ending at −0.30 V vs RHE with a scan rate of 5 mV/s. Throughout these measurements, the electrolyte was purged with H_2 gas, and the working electrode was rotated at 1600 rpm in the RDE to remove hydrogen gas bubbles formed at the catalyst surface.

To measure electrochemical capacitance, the potential was swept from 0.15 to 0.35 V and back to 0.15 V three times at each of six different scan rates (10, 20, 40, 80, 160, and 320 mV/s). The working electrode was held at each potential vertex for 20 s before beginning the next sweep. These scans were performed on the molybdenum sulfide catalyst while purging with N_2 gas and rotating at 1600 rpm in the RDE. The rate of rotation was observed to have no effect on the measured capacitive current. The same set of scans was also performed on a flat standard MoS_2 sample (preparation details provided in the Supporting Information) in a compression cell with a N_2 gas purge and no rotation.

Extended potential cycling was performed to investigate changes in composition during catalysis and to evaluate the catalyst's durability. These tests were performed by taking linear sweep voltammograms after repeatedly cycling the potential between 0.10 and −0.25 V vs RHE at 50 mV/s. The first 20 potential cycles were performed at 0 rpm, and the next 5 cycles were performed at 1600 rpm. This pattern was repeated three additional times. Performing the majority of the cycles at 0 rpm prevented the RDE apparatus from overheating due to prolonged continuous rotation, and periodic rotation still enabled removal of H_2 bubbles. After every 100 potential cycles, the potential was swept from 0.10 to −0.30 V vs RHE at 5 mV/s and 1600 rpm. The slow scans were used to minimize contributions from capacitance current and obtain a more accurate measure of the electrochemical activity. For electrochemical stability testing, this program was repeated 100 times for 10 000 total potential cycles at 50 mV/s (approximately

48 h). The samples prepared for X-ray photoelectron spectroscopy measurements were cycled using this program for 4 h. A continual H_2 gas purge was used for the duration of these tests. As appropriate, these samples were rinsed in Millipore water to remove any residual sulfuric acid prior to spectroscopic measurements.

■ RESULTS AND DISCUSSION

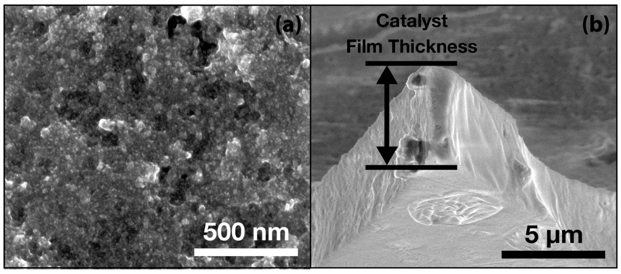

Figure 1. SEM images showing (a) the catalyst film surface morphology and (b) a thickness cross section of a segment of the catalyst film that delaminated from the substrate surface.

The morphology of the catalyst film was characterized using scanning electron microscopy, as shown in Figure 1. The film has a rough, nanostructured surface with feature sizes ranging from 50 to 100 nm. This structure arises from the agglomeration of the catalyst nanoparticles upon drop-casting and is favorable for catalysis because it provides a high surface area interface between the catalyst and the electrolyte, which is conducive to high overall electrochemical activity. An image of a portion of the catalyst film that delaminated from the substrate shows that the film is ~5−7 μm thick, assuming an observation angle between 0° and 45° with respect to the film surface. The amount of catalyst on the substrate is greater than the typical loading for precious metal electrocatalysts, which are often deposited as isolated nanoparticles rather than as a porous film.[5,35,36] However, due to the low material cost and straightforward synthetic procedure of the molybdenum sulfide catalyst, this film structure could potentially be practical for wide-scale deployment.

The crystallinity of the film was investigated before electrochemical characterization using TEM and XRD. TEM of an isolated nanoparticle (Figure 2) shows that the diameter of the catalyst particle is ~60 nm, which corresponds to the size of the features observed using SEM after the particles agglomerate into the rough, nanostructured film morphology. The absence of lattice or Moiré fringes observed in the bright field TEM image suggests that the material is amorphous, which was further confirmed by the lack of any XRD peaks that would suggest a crystalline catalyst film (see Supporting Information Figure S1). Raman spectroscopy revealed the absence of the distinctive A_{1g} and E^1_{2g} vibrational peaks expected for crystalline MoS_2 (see Supporting Information Figure S2), which suggests that crystalline MoS_2 is not present in significant quantities in the as-deposited catalyst.[37−39]

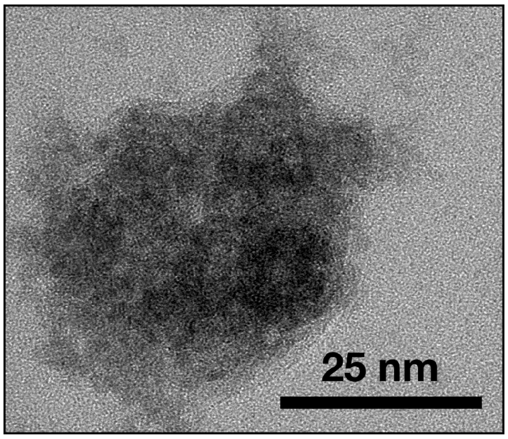

Figure 2. Transmission electron micrograph of an isolated particle deposited from a diluted molybdenum sulfide catalyst suspension.

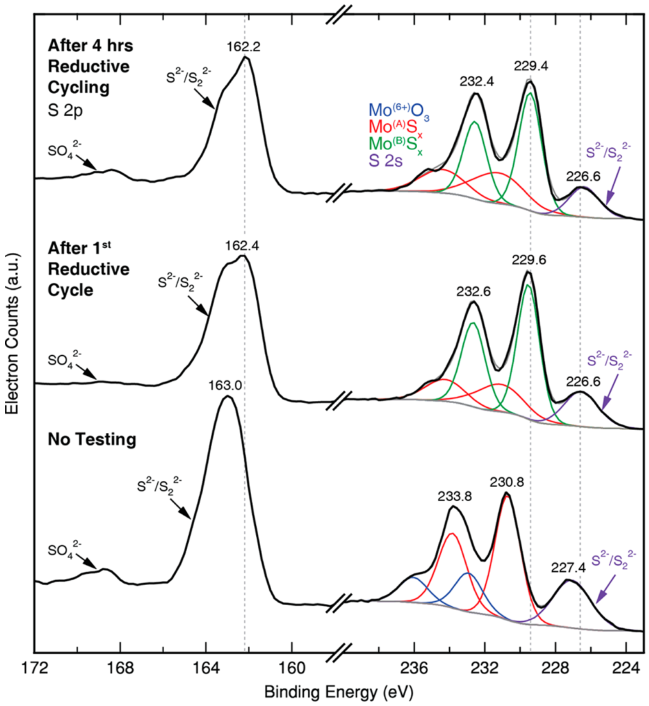

Figure 3. X-ray photoelectron spectra of the catalyst surface before testing, after one reductive potential cycle, and after 4 h of continuous reductive cycling. The data are scaled to normalize the Mo 3d peak areas. Before electrochemical testing, the shape and binding energy of the S 2p peak are indicative of amorphous MoS_3. The Mo 3d peaks show that the majority of the molybdenum occurs in chemical state $Mo^{(A)}S_x$. The peak positions and shapes begin to change after the initial reductive potential cycle, corresponding to the catalyst activation observed during electrochemical testing. These changes are accentuated after extended electrochemical testing. In the tested samples, the S 2p peak shape and binding energy more closely resemble MoS_2, and the majority of the molybdenum occurs in chemical state $Mo^{(B)}S_x$, with binding energies near the Mo 4+ peaks observed in MoS_2.

X-ray photoelectron spectra collected before electrochemical testing (Figure 3) show that the as-deposited ("no testing") material resembles molybdenum trisulfide (MoS_3). The sulfur 2p region shows a peak at a binding energy of 163.0 eV, with a broad full width at half-maximum (fwhm) of 2.2 eV and no evidence of the expected spin−orbit splitting doublet corresponding to the $2p_{1/2}$ and $2p_{3/2}$ lines, which suggests that the sulfur atoms near the surface exist in multiple oxidation states. These observations are consistent with previous reports of MoS_3 materials, which contain sulfur in a combination of S_2^{2-} and S^{2-} groups.[11,29,34,40,41] A small peak observed near 169 eV corresponds to the binding energy of sulfur in a sulfate group[42,43] and likely arises from residual SO_4^{2-} from the sulfuric acid used in the catalyst synthesis. The presence of small nitrogen 1s and sodium 1s peaks indicates that there may also be some residual Na^+ and NH_4^+ from the catalyst synthesis, but these peaks disappear after the catalyst has been immersed in water or sulfuric acid (see Supporting Information Figure S3).

The molybdenum 3d region reveals a mixture of Mo oxidation states. Peak fitting shows that ~ 27% of the Mo signal corresponds to a 6+ oxidation state. XPS spectra of an untested catalyst sample aged in air show that this feature arises primarily from oxidation to form a thin layer of $Mo^{(6+)}O_3$ (see Supporting Information Figure S4). The remaining 73% of the Mo signal arises from the molybdenum sulfide. This Mo exists in a chemical state labeled here as $Mo^{(A)}S_x$, which likely corresponds to a lower oxidation state of either 4+ or 5+. The amorphous structure of this material prohibits the definitive determination of the formal oxidation state, as the observed binding energies are likely influenced by a number of factors, including the oxidation state, sulfur coordination, and local bonding structure. To quantify the Mo and S components of the molybdenum sulfide film, the peak areas pertaining to the Mo 3d and the sulfide/persulfide S 2p lines were measured and calibrated versus a reference scan of a natural MoS_2 crystal, which served as a standard (see Supporting Information Figure S5). This analysis reveals that the composition near the catalyst surface (~3 nm probe depth) is 22% Mo and 78% S as-synthesized (disregarding the S pertaining to sulfate as well as all other elements). These values closely match the 25% Mo and 75% S expected for molybdenum trisulfide. Thus, the atomic composition and binding energies measured by XPS and the amorphous structure observed by TEM and XRD suggest that the as-deposited material is predominantly composed of amorphous MoS_3.[40,41,44−53]

We investigated the electrochemical properties of the molybdenum sulfide catalyst using a three-electrode electrochemical cell in a rotating disk electrode configuration. Catalyst activation is observed upon the first reductive potential cycle (Figure 4). Initially, the onset of reductive current is observed near −200 mV vs RHE, but after completing the first potential cycle, the onset of reductive current shifts to approximately −150 mV vs RHE and remains stable in subsequent cycles. The current observed on the first reductive cycle is likely a combination of hydrogen evolution and electrochemical reduction of the catalyst material to form the catalytically active phase, the nature of which is discussed below. A similar reductive activation was also observed in other recent studies of amorphous molybdenum sulfide HER catalyst materials.[29,34]

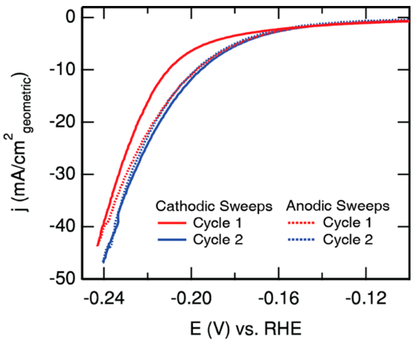

Figure 4. Cyclic voltammograms indicate that the molybdenum sulfide catalyst is activated during the cathodic sweep of the first cycle (solid red line). Enhanced activity is observed on the anodic sweep of the first cycle (dotted red line) and in subsequent cycles (blue lines).

A polarization curve demonstrating the HER activity of the molybdenum sulfide catalyst on a glassy carbon electrode is compared with a bare glassy carbon control in Figure 5a. The catalyst shows high activity for the HER with ~200 mV overpotential necessary to achieve 10 mA/cm^2 hydrogen evolution current density, which is a useful metric for comparing catalysts for solar hydrogen production.[5,54] Measurements performed on four duplicate samples show consistent activity, with the overpotentials necessary to achieve 10 mA/cm^2 current density ranging from 198 to 204 mV (see Supporting Information Figure S6).

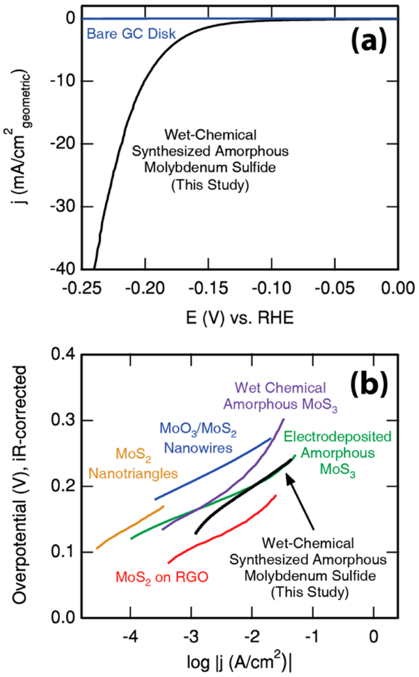

Figure 5. Electrochemical activity of the molybdenum sulfide catalyst. Polarization curves (a) show that the catalyst exhibits high activity for the HER. A Tafel plot (b) shows the electrochemical activity of the wet-chemical-synthesized amorphous molybdenum sulfide catalyst along with digitized data of HER measurements of several other materials for comparison, including MoS_2 nanotriangles in pH 0.24 H_2SO_4 (orange trace),[24] MoO_3/MoS_2 core−shell nanowires in 0.5 M H_2SO_4 (blue trace),[27] electrodeposited amorphous MoS_3 in pH 0 electrolyte (green trace),[29] wet chemical synthesized amorphous MoS_3/multiwalled carbon nanotube composite in 1 M H_2SO_4 (purple trace),[34] and MoS_2 on reduced graphene oxide in 0.5 M H_2SO_4 (red trace).[28]

The activity of the wet-chemical-synthesized amorphous molybdenum sulfide catalyst is compared with several other MoS_2 and MoS_3 materials in the Tafel plot shown in Figure 5b.[27−29,32,34] This material shows the highest activity of any reported molybdenum sulfide catalyst synthesized using a room temperature wet chemical procedure. The activity is within ~50 mV of the best reported molybdenum sulfide catalyst synthesized using any technique.[28] The average Tafel slope for this catalyst is 60 mV/decade, with individual slopes ranging from 53 to 65 mV/decade for the catalyst films shown in Figures 5 and Supporting Information S6. Although the Tafel slope alone is insufficient to determine the specific mechanism of the HER,[27,55,56] it does match several earlier reports for molybdenum sulfide catalysts, which also exhibited slopes of ~60 mV/decade.[27,32]

To understand the changes in the material during electrochemical testing and identify the active form of the catalyst, we performed XPS after catalyst activation via the first reductive potential cycle and after 4 h of continuous reductive cycling (Figure 3). XPS spectra collected after electrochemical testing reveal pronounced changes in the material, both in the elemental ratio and in the chemical states of the Mo and S. The S 2p peak corresponding to the catalyst material after the initial activation cycle shifts from 163.0 to 162.4 eV and begins to resemble a single spin−orbit splitting doublet. After 4 h of reductive cycling, the S 2p region displays a distinct spin−orbit splitting doublet with the S $2p_{3/2}$ peak at a binding energy of 162.2 eV, very close to the value observed in crystalline MoS_2 (see Supporting Information Figure S5). The same can be said for the S 2s line, which shifts from 227.4 eV before testing to 226.2 eV after testing, the binding energy observed in crystalline MoS_2. This trend suggests that the sulfur in the sample is partially reduced during catalysis and the dominant form of sulfur present after testing exists in a chemical environment similar to MoS_2.

Significant changes are also observed in the Mo 3d region after electrochemical testing. First, the amount of $Mo^{(6+)}O_3$ has decreased substantially to a negligible quantity that obviates the need for fitted features in the deconvoluted spectra of the “after testing” samples in Figure 3; thus, for the sake of clarity, those particular features are omitted. This significant decrease in $Mo^{(6+)}O_3$ was also observed in catalyst samples allowed to rest in water or 0.5 M H_2SO_4 with no applied potential, so we attribute this difference to the chemical dissolution of the native surface oxide (see Supporting Information Figure S7). This observation is consistent with the expectation that any MoO_3 would dissolve in the electrolyte used during catalyst testing.[27,57] The second noticeable change is a significant shift in the binding energies of the Mo peaks corresponding to the molybdenum sulfide. Prior to testing, the majority of the molybdenum exists as $Mo^{(A)}S_x$. After the initial activation and after 4 h of reductive cycling, the majority of the near-surface molybdenum is found in a slightly more reduced state labeled here as $Mo^{(B)}S_x$, with $3d_{3/2}$ and $3d_{5/2}$ peaks near 232.6 and 229.5 eV, respectively. Approximately one-third of the Mo remains as $Mo^{(A)}S_x$ in both cases. A small amount of $Mo^{(6+)}O_3$ may be hidden within the $Mo^{(A)}S_x$ peaks, causing them to appear at a slightly higher binding energy than observed before catalytic testing. The shift from $Mo^{(A)}S_x$ to $Mo^{(B)}S_x$ corresponds to a change in chemical environment, and the direction of this shift is consistent with a reduction of the molybdenum, as expected based on the reductive potentials applied during catalyst activation and HER catalysis. The Mo $3d_{3/2}$ and $3d_{5/2}$ binding energies in the $Mo^{(B)}S_x$ are close to the values observed in crystalline MoS_2 (see Supporting Information Figure S5), which has a Mo oxidation state of 4+. The small remaining difference in the binding energies may arise from the different sulfur coordination or local bonding structure in this catalyst. All the changes in the molybdenum spectra measured after catalysis show that the active form of the catalyst resembles MoS_2, although it is likely not a pure phase, since the Mo still exists in multiple chemical states.

Finally, quantification of the Mo and sulfide/persulfide S signals after catalysis reveals changes in the stoichiometry of the near-surface region. After the initial reductive cycle, the sample’s composition has changed from 22% Mo and 78% S (consistent with molybdenum trisulfide) to a composition of 34% Mo and 66% S, closely matching the 33% Mo and 67% S expected in MoS_2. After four hours of reductive cycling, the composition appears to have continued to change, albeit slightly, to 39% Mo and 61% S. These values, which are also within experimental error of MoS_2, could suggest a subtle depletion of sulfur during catalysis. All of these observations regarding the quantification and chemical state of Mo and S suggest that the MoS_3 material resulting from the wet chemical synthesis could be considered a “precatalyst.” This material undergoes major changes during operation to create the active phase, which more closely resembles MoS_2, consistent with the trends observed in previous reports of amorphous MoS_3 materials.[29,34] However, Raman spectra collected after catalysis (see Supporting Information Figure S2) confirm that the sample still does not contain crystalline MoS_2 in a detectable quantity. Therefore, the reduced phase created during catalysis is likely an amorphous MoS_2.

Because of the amorphous and nanostructured nature of this catalyst, there is likely significant surface site heterogeneity in this material. It is therefore difficult to accurately determine the structure and relative concentration of various types of surface sites, which makes the identification of the active sites of this material particularly challenging. Previous work on many different types of molybdenum sulfide materials shows that this general class of catalyst can exhibit high activity for hydrogen evolution, despite wide variations in atomic structure and chemical composition.[11,23,25,27−32,34,58] The catalyst material presented in this work likely exhibits many types of surface sites due to its amorphous, nanostructured nature, some of which could resemble the active sites previously described in the studies cited above. It is therefore possible that many different types of surface sites participate in the reaction. The results of this study provide initial indications that domains resembling MoS_2 are created during catalysis and may contribute to this material’s high electrochemical activity, but further characterization is necessary to confirm this hypothesis. Synchrotron techniques such as X-ray absorption spectroscopy could yield greater insights about the catalyst composition and structure.[11,49]

The intrinsic per-site activity of a catalyst is an important metric necessary to compare catalyst materials and to guide catalyst development. To estimate this key figure of merit, we used electrochemical capacitance surface area measurements to determine the active surface area of the catalyst film.[59,60] When combined with a simplified model of the surface structure (details provided in the Supporting Information), this technique enables independent estimation of the density of electrochemically active sites and the average activity of each site, reported as a per-site turnover frequency (TOF). Although the analysis shown here utilizes known properties for MoS_2, which may not perfectly reflect MoS_3 or the reduced phase created during electrochemical testing, it nevertheless provides useful insights for future improvements to catalyst design.

To find the electrochemically active surface area, as shown in Figure 6a, we measured the non-faradic capacitive current associated with electrochemical double layer charging upon repeated potential cycling. This double layer charging current, i_c, is proportional to both the scan rate, ν, and the electrochemically active surface area of the electrode, A_{echem}:[61]

$$i_c \propto \nu \times A_{echem}$$

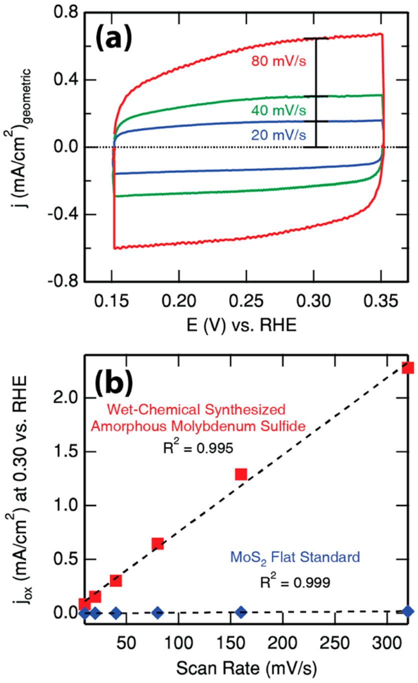

Figure 6. Electrochemical capacitance measurements for determination of the molybdenum sulfide catalyst surface area. Cyclic voltammograms (a) were taken in a potential range where no faradic processes were observed to measure the capacitive current from double layer charging. The capacitive current measured at 0.30 V vs RHE was plotted as a function of scan rate (b) for the wet-chemical-synthesized amorphous molybdenum sulfide and the MoS_2 flat standard. The ratio of the capacitive currents for the molybdenum sulfide catalyst and the flat standard was used to determine the relative roughness factor.

The capacitive currents for the molybdenum sulfide catalyst and for a flat MoS_2 standard (preparation details provided in the Supporting Information) were measured as a function of scan rate, as shown in Figure 6b. A potential range of 0.15−0.35 V vs RHE was selected for the capacitance measurements because no obvious electrochemical features corresponding to faradic current were observed in this region. Furthermore, the dependence of the current on the scan rate in this region is linear for both materials, which is consistent with capacitive charging behavior. Current arising from a faradic process would yield a square root dependence with respect to scan rate as a result of mass transfer (reactant diffusion) limitations.[62] The ratio of the currents for the catalyst and the flat MoS_2 standard was taken as the relative roughness factor, RF:

$$\mathrm{RF} = \frac{i_c(\text{catalyst})}{i_c(\text{flat standard})} = \frac{\text{catalyst active surface area}}{\text{substrate geometric surface area}}$$

From this analysis, we measured a RF value of 90. This calculation relies on the assumption that the intrinsic, surface-area-normalized capacitance of the molybdenum sulfide catalyst and the flat MoS_2 standard are the same. Although the chemical and physical characteristics of MoS_2 differ from the amorphous molybdenum sulfide catalyst, we chose to use a MoS_2 flat standard due to the difficulty of fabricating a perfectly flat, well-defined analogue of the amorphous molybdenum sulfide catalyst. The capacitance measured for the flat MoS_2, approximately 60 μF/cm^2, is consistent with expectations for a flat electrode.[59,62] Because the surface-area-normalized capacitance associated with double layer charging is expected to be similar (i.e., within an order of magnitude) for many metallic and semiconducting materials in the same aqueous electrolyte,[62] the resulting surface area estimate for our work presented here is accurate to within an order of magnitude or better.

The RF was used to estimate the density of electrochemically accessible sites on the catalyst surface, ~10^{17}/cm^2 of geometric electrode area (calculation details are provided in the Supporting Information). Using this surface site density, we calculated a turnover frequency (TOF) of 0.3 H_2/s per surface site at 200 mV overpotential (~10 mA/cm^2 of current density, calculated per geometric electrode area). Conservatively, because of the order of magnitude inaccuracy of these calculations, the TOF may fall between 0.03 H_2/s and 3 H_2/s per surface site. This range is comparable to the TOFs reported for other highly active molybdenum sulfide catalysts at similar current densities.[27,29] However, previous reports of well-defined MoS_2 nanoparticles indicate that the intrinsic TOF for a crystalline MoS_2 edge site is ~3 orders of magnitude higher.[27,32] As discussed previously, there is likely significant surface site heterogeneity in this amorphous molybdenum sulfide material, which raises the possibility that only a fraction of the surface sites may be active for hydrogen evolution. Therefore, the true TOF of the most active sites could be orders of magnitude greater than the average value of 0.3 H_2/s.

In any event, the high surface area nanostructured morphology of the catalyst film clearly plays an important role in providing a significant number of active sites. To further investigate the effect of electrochemically active surface area on the observed activity, we synthesized samples with mass loadings varying from 25% to 400% of the typical catalyst preparation. As shown in Figure 7, we found that the activity of these samples, as measured by the overpotential needed to reach 1 mA/cm^2 on a geometric area basis, varies linearly with log(RF). This shows that increasing surface area translates to improved activity in a predictable manner based on standard models of electrochemical kinetics. Note, however, that the slope of the regression line, 38 mV/decade, is slightly lower than the expected value of 60 mV/decade based on the Tafel analysis described earlier. This difference may result from limitations from mass transport or charge transport for thicker, higher surface area films. Ultimately, the linearity of the data provides additional evidence that the high surface area morphology of the catalyst film contributes significantly to its high activity and may explain, in part, why this catalyst has

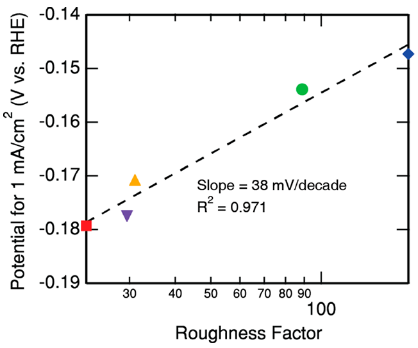

Figure 7. Electrochemical activity of catalyst samples as a function of roughness factor. The catalyst activity increases linearly with the log of the roughness factor.

activity superior to similar materials reported previously[29,34] (additional discussion is presented in the Supporting Information along with further electrochemical data in Figure S8 and SEM images in Figure S9). This result suggests that high catalytic current densities could be achieved from a much lower catalyst loading by depositing the molybdenum sulfide catalyst onto a high surface area support.[27] Similarly, the activity of this catalyst could be further improved by increasing the roughness factor beyond 90.

The long-term stability of a catalyst is another important metric to consider for commercial applications. The stability of this catalyst film was assessed by repeated potential cycling for more than 10 000 cycles to replicate diurnal cycling experienced by a HER catalyst for solar water splitting. The lower bound of the potential cycles, −0.25 V vs RHE, was chosen to reach a current density in excess of 10 mA/cm^2, which is a useful metric for comparing catalysts for solar hydrogen production. The results of the stability testing are displayed in Figure 8, which shows that the overpotential required to attain 10 mA/cm^2 current density increases by only 57 mV after 10 000 potential cycles. Although not quite as stable as some other molybdenum sulfide materials,[27,28] the absolute overpotential required to drive 10 mA/cm^2 remains low.

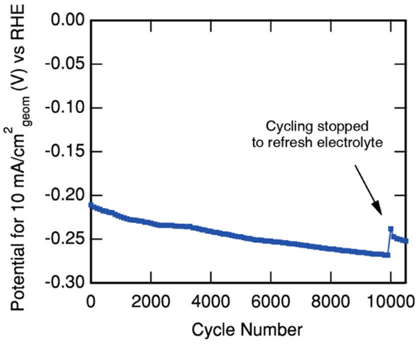

Figure 8. Electrochemical stability of the molybdenum sulfide catalyst. The overpotential required to reach a current density of 10 mA/cm^2 increases by only 57 mV after 10 000 reductive potential cycles, indicating that the catalyst remains highly active.

Several factors may contribute to the slight loss in activity. One hypothesis is that surface adsorbates, potentially from impurities in the electrolyte, reference electrode, or within the film itself, may poison the active sites of the catalyst over the course of the stability testing. We tested this hypothesis by pausing the stability testing after the 10 000th cycle to replace the electrolyte solution, after which the catalyst immediately recovered 30 mV of activity during subsequent measurements. Delamination of the catalyst film from the substrate is another likely cause of activity loss, an effect confirmed by scanning electron microscope imaging performed after electrochemical testing (see Supporting Information Figure S10). This loss of catalyst loading could potentially be remedied by using a conductive binder to secure the catalyst to the glassy carbon substrate or by depositing this material upon a different substrate altogether. Although further study is required to detail the specific mechanisms of the catalyst degradation, our preliminary efforts indicate that factors other than the inherent properties of the catalyst material are responsible for the observed decrease in activity. Overall, this highly active material remains an excellent HER catalyst throughout the course of the rigorous accelerated durability test.

■ CONCLUSIONS

We have developed a scalable wet chemical synthesis to produce a highly active, stable, amorphous molybdenum sulfide HER electrocatalyst. This synthetic technique requires no high-temperature processing or secondary sulfidization step and allows for direct catalyst deposition onto many types of substrates. We performed extensive spectroscopic and electrochemical characterization to understand changes in this material during catalysis and investigate the origin of the catalytic activity of amorphous molybdenum sulfide catalysts, for which there have been several recent literature reports. Domains resembling MoS_2 in both composition and chemical state are created during catalysis and may contribute to the high HER activity of this material. The high density of active sites that results from the rough, nanostructured surface morphology also contributes to the high geometric current densities. The catalyst's stability was also ascertained; it was found to retain its activity throughout extended reductive potential cycling. The catalyst activity and stability could be further improved by designing a substrate structure to increase the total surface area and prevent catalyst delamination during operation. This highly active, stable HER catalyst is a promising candidate material that could help to enable the widespread deployment of cost-effective systems for electrochemical hydrogen production.

■ ASSOCIATED CONTENT

Ⓢ Supporting Information

Experimental details, additional XPS spectra, XRD spectra, Raman spectra, electrochemical activity of duplicate samples, additional SEM images of the catalyst films, electrochemical activity variation with mass loading, and TOF calculation details. This material is available free of charge via the Internet at http://pubs.acs.org.

■ AUTHOR INFORMATION

Corresponding Author

*Phone: 650-498-6879. E-mail: jaramillo@stanford.edu.

Notes

The authors declare no competing financial interest.

■ ACKNOWLEDGMENTS

This work was supported as part of the Center on Nanostructuring for Efficient Energy Conversion (CNEEC) at Stanford University, an Energy Frontier Research Center funded by the U.S. Department of Energy, Office of Science, Office of Basic Energy Sciences under Award No. DE-SC0001060. J.D.B. acknowledges support from the National Science Foundation Graduate Research Fellowship Program and a Stanford Graduate Fellowship. A.J.F. was supported by the U.S. Department of Energy, Office of Energy Efficiency and Renewable Energy, under Subcontract NFT-9-88567-01 under prime Contract No. DE-AC36-08GO28308. The authors thank Benjamin Reinecke for performing the TEM imaging, Andrey Malkovskiy for help with Raman spectroscopy, and Yelena Gorlin for helpful discussions about electrochemical stability measurements.

■ REFERENCES

(1) Häussinger, P.; Lohmüller, R.; Watson, A. M. Hydrogen, 6. Uses. In *Ullmann's Encyclopedia of Industrial Chemistry*; Wiley-VCH Verlag GmbH & Co. KGaA: Weinheim, 2000.

(2) U.S. Energy Information Administration. The Impact of Increased Use of Hydrogen on Petroleum Consumption and Carbon Dioxide Emissions. http://www.eia.gov/oiaf/servicerpt/hydro/pdf/oiafcneaf%2808%2904.pdf (accessed August 5, 2012).

(3) Turner, J. A. *Science* **2004**, *305* (5686), 972−974.

(4) Nowotny, J.; Sorrell, C. C.; Sheppard, L. R.; Bak, T. *Int. J. Hydrogen Energy* **2005**, *30* (5), 521−544.

(5) Walter, M. G.; Warren, E. L.; McKone, J. R.; Boettcher, S. W.; Mi, Q. X.; Santori, E. A.; Lewis, N. S. *Chem. Rev.* **2010**, *110* (11), 6446−6473.

(6) Cook, T. R.; Dogutan, D. K.; Reece, S. Y.; Surendranath, Y.; Teets, T. S.; Nocera, D. G. *Chem. Rev.* **2010**, *110* (11), 6474−6502.

(7) Turner, J.; Sverdrup, G.; Mann, M. K.; Maness, P. C.; Kroposki, B.; Ghirardi, M.; Evans, R. J.; Blake, D. *Int. J. Energy Res.* **2008**, *32* (5), 379−407.

(8) Bak, T.; Nowotny, J.; Rekas, M.; Sorrell, C. C. *Int. J. Hydrogen Energy* **2002**, *27* (10), 991−1022.

(9) Kibler, L. A. *ChemPhysChem* **2006**, *7* (5), 985−991.

(10) Subbaraman, R.; Tripkovic, D.; Strmcnik, D.; Chang, K.-C.; Uchimura, M.; Paulikas, A. P.; Stamenkovic, V.; Markovic, N. M. *Science* **2011**, *334* (6060), 1256−1260.

(11) Tang, M. L.; Grauer, D. C.; Lassalle-Kaiser, B.; Yachandra, V. K.; Amirav, L.; Long, J. R.; Yano, J.; Alivisatos, A. P. *Angew. Chem., Int. Ed.* **2011**, *50* (43), 10203−10207.

(12) Krstajic, N. V.; Jovic, V. D.; Gajic-Krstajic, L.; Jovic, B. M.; Antozzi, A. L.; Martelli, G. N. *Int. J. Hydrogen Energy* **2008**, *33* (14), 3676−3687.

(13) Lasia, A.; Rami, A. *J. Electroanal. Chem.* **1990**, *294* (1−2), 123−141.

(14) Rami, A.; Lasia, A. *J. Appl. Electrochem.* **1992**, *22* (4), 376−382.

(15) Machado, S. A. S.; Avaca, L. A. *Electrochim. Acta* **1994**, *39* (10), 1385−1391.

(16) Petrov, Y.; Schosger, J.-P.; Stoynov, Z.; de Bruijn, F. *Int. J. Hydrogen Energy* **2011**, *36* (20), 12715−12724.

(17) Endoh, E.; Otouma, H.; Morimoto, T.; Oda, Y. *Int. J. Hydrogen Energy* **1987**, *12* (7), 473−479.

(18) Huq, A. K. M. S.; Rosenberg, A. J.; Makrides, A. C. *J. Electrochem. Soc.* **1964**, *111* (3), 278−286.

(19) Birry, L.; Lasia, A. *J. Appl. Electrochem.* **2004**, *34* (7), 735−749.

(20) Dominey, R. N.; Lewis, N. S.; Bruce, J. A.; Bookbinder, D. C.; Wrighton, M. S. *J. Am. Chem. Soc.* **1982**, *104* (2), 467−482.

(21) Li, Y.; Somorjai, G. A. *Nano Lett.* **2010**, *10* (7), 2289−2295.

(22) Boettcher, S. W.; Spurgeon, J. M.; Putnam, M. C.; Warren, E. L.; Turner-Evans, D. B.; Kelzenberg, M. D.; Maiolo, J. R.; Atwater, H. A.; Lewis, N. S. *Science* **2010**, *327* (5962), 185−187.

(23) Hou, Y. D.; Abrams, B. L.; Vesborg, P. C. K.; Bjorketun, M. E.; Herbst, K.; Bech, L.; Setti, A. M.; Damsgaard, C. D.; Pedersen, T.; Hansen, O.; Rossmeisl, J.; Dahl, S.; Norskov, J. K.; Chorkendorff, I. *Nat. Mater.* **2011**, *10* (6), 434−438.

(24) Jaramillo, T. F.; Jorgensen, K. P.; Bonde, J.; Nielsen, J. H.; Horch, S.; Chorkendorff, I. *Science* **2007**, *317* (5834), 100−102.

(25) Jaramillo, T. F.; Bonde, J.; Zhang, J. D.; Ooi, B. L.; Andersson, K.; Ulstrup, J.; Chorkendorff, I. *J. Phys. Chem. C* **2008**, *112* (45), 17492−17498.

(26) Bonde, J.; Moses, P. G.; Jaramillo, T. F.; Norskov, J. K.; Chorkendorff, I. *Faraday Discuss.* **2008**, *140*, 219−231.

(27) Chen, Z. B.; Cummins, D.; Reinecke, B. N.; Clark, E.; Sunkara, M. K.; Jaramillo, T. F. *Nano Lett.* **2011**, *11* (10), 4168−4175.

(28) Li, Y. G.; Wang, H. L.; Xie, L. M.; Liang, Y. Y.; Hong, G. S.; Dai, H. J. *J. Am. Chem. Soc.* **2011**, *133* (19), 7296−7299.

(29) Merki, D.; Fierro, S.; Vrubel, H.; Hu, X. L. *Chem. Sci.* **2011**, *2* (7), 1262−1267.

(30) Merki, D.; Hu, X. *Energy Environ. Sci.* **2011**, *4* (10), 3878−3888.

(31) Laursen, A. B.; Kegnaes, S.; Dahl, S.; Chorkendorff, I. *Energy Environ. Sci.* **2012**, *5*, 2.

(32) Jaramillo, T. F.; Jorgensen, K. P.; Bonde, J.; Nielsen, J. H.; Horch, S.; Chorkendorff, I. *Science* **2007**, *317* (5834), 100−102.

(33) Merki, D.; Vrubel, H.; Rovelli, L.; Fierro, S.; Hu, X. *Chem. Sci.* **2012**, *3* (8), 2515−2525.

(34) Vrubel, H.; Merki, D.; Hu, X. *Energy Environ. Sci.* **2012**, *5* (3), 6136−6144.

(35) Gilliam, R.; Kirk, D.; Thorpe, S. *Electrocatalysis* **2012**, *3*, 1−7.

(36) Gasteiger, H. A.; Kocha, S. S.; Sompalli, B.; Wagner, F. T. *Appl. Catal., B* **2005**, *56* (1−2), 9−35.

(37) Eda, G.; Yamaguchi, H.; Voiry, D.; Fujita, T.; Chen, M.; Chhowalla, M. *Nano Lett.* **2011**, *11* (12), 5111−5116.

(38) Lee, C.; Yan, H.; Brus, L. E.; Heinz, T. F.; Hone, J.; Ryu, S. *ACS Nano* **2010**, *4* (5), 2695−2700.

(39) Wieting, T. J.; Verble, J. L. *Phys. Rev. B* **1971**, *3* (12), 4286−4292.

(40) Weber, T.; Muijsers, J. C.; Niemantsverdriet, J. W. *J. Phys. Chem.* **1995**, *99* (22), 9194−9200.

(41) Iranmahboob, J.; Gardner, S. D.; Toghiani, H.; Hill, D. O. *J. Colloid Interface Sci.* **2004**, *270* (1), 123−126.

(42) Wagner, C. D.; Taylor, J. A. *J. Electron Spectrosc. Relat. Phenom.* **1980**, *20* (1−2), 83−93.

(43) Siriwardane, R. V.; Cook, J. M. *J. Colloid Interface Sci.* **1986**, *114* (2), 525−535.

(44) Jacobson, A. J.; Chianelli, R. R.; Rich, S. M.; Whittingham, M. S. *Mater. Res. Bull.* **1979**, *14* (11), 1437−1448.

(45) Liang, K. S.; Cramer, S. P.; Johnston, D. C.; Chang, C. H.; Jacobson, A. J.; Deneufville, J. P.; Chianelli, R. R. *J. Non-Cryst. Solids* **1980**, *42* (1−3), 345−356.

(46) Chang, C. H.; Chan, S. S. *J. Catal.* **1981**, *72* (1), 139−148.

(47) Bhattacharya, R. N.; Lee, C. Y.; Pollak, F. H.; Schleich, D. M. *J. Non-Cryst. Solids* **1987**, *91* (2), 235−242.

(48) Belanger, D.; Laperriere, G.; Marsan, B. *J. Electroanal. Chem.* **1993**, *347* (1−2), 165−183.

(49) Hibble, S. J.; Rice, D. A.; Pickup, D. M.; Beer, M. P. *Inorg. Chem.* **1995**, *34* (21), 5109−5113.

(50) Hibble, S. J.; Walton, R. I.; Pickup, D. M.; Hamon, A. C. *J. Non-Cryst. Solids* **1998**, *232*, 434−439.

(51) Hibble, S. J.; Feaviour, M. R.; Almond, M. J. *J. Chem. Soc., Dalton Trans.* **2001**, *6*, 935−940.

(52) Jiao, H. J.; Li, Y. W.; Delmon, B.; Halet, J. F. *J. Am. Chem. Soc.* **2001**, *123* (30), 7334−7339.

(53) Hibble, S. J.; Wood, G. B. *J. Am. Chem. Soc.* **2004**, *126* (3), 959−965.

(54) Weber, M. F.; Dignam, M. J. *J. Electrochem. Soc.* **1984**, *131* (6), 1258−1265.

(55) Markovic, N. M.; Grgur, B. N.; Ross, P. N. *J. Phys. Chem. B* **1997**, *101* (27), 5405−5413.

(56) Sheng, W.; Gasteiger, H. A.; Shao-Horn, Y. *J. Electrochem. Soc.* **2010**, *157* (11), B1529−B1536.

(57) Pourbaix, M., *Atlas of Electrochemical Equilibria in Aqueous Solutions*, 2nd ed.; NACE International: Houston, TX, 1974.

(58) Karunadasa, H. I.; Montalvo, E.; Sun, Y. J.; Majda, M.; Long, J. R.; Chang, C. J. *Science* **2012**, *335* (6069), 698−702.

(59) Kotz, R.; Carlen, M. *Electrochim. Acta* **2000**, *45* (15−16), 2483−2498.

(60) Trasatti, S.; Petrii, O. A. *Pure Appl. Chem.* **1991**, *63* (5), 711−734.

(61) Bard, A. J.; Faulkner, L. R. *Electrochemical Methods: Fundamentals and Applications*; Wiley: New York, 2001.

(62) Conway, B. E.; Birss, V.; Wojtowicz, J. *J. Power Sources* **1997**, *66* (1−2), 1−14.